The mechanism of sonophotocatalytic degradation of methyl orange and its products in aqueous solutions

Yuanhua He, Franz Grieser, Muthupandian Ashokkumar *

Particulate Fluid Processing Center, School of Chemistry, University of Melbourne, Parkville, VIC. 3010, Australia

ARTICLE INFO

ABSTRACT

In this study, it was found that a hybrid technique, sonophotocatalysis, is able to degrade a parent organic pollutant (methyl orange) as well as its by-products. The analysis of products formed during the whole degradation has demonstrated that the pH or the selection of oxidation process (sonolysis/photocatalysis/sonophotocatalysis) is able to control the degradation pathway. It was shown in the by-products analysis that the solution pH can alter the amount of each product generated during the sonophotocatalytic degradation. It was revealed that the different degradation rates of methyl orange and its products result from the solution pH and the nature of the organic products. Furthermore, a comparison of the data obtained from the oxidation processes on the degradation of the reaction intermediates identified the advantages of the combined system. It is concluded that sonophotocatalysis is capable of yielding a more complete and faster mineralization of organic pollutants than the individual processes. However, as in the degradation of the parent compound, the overall mineralization is lower than an additive effect (negative synergistic effect).

© 2011 Elsevier B.V. All rights reserved.

1. Introduction

Although both photocatalytic [1–4] and sonolytic [5–8] degradation of organic pollutants have been found to be useful in the remediation of environmental contaminants, the critical limit for these individual processes is their relatively low efficiency for the complete mineralization of organic pollutants. Some considerable effort has been directed at enhancing the efficacy of advanced oxidation processes (AOPs) by forming hybrid systems from two or more techniques [7,9–12].

A number of research groups have examined the combination of ultrasound and photocatalysis, known as sonophotocatalysis (SPC), for environmental remediation [7,10–15]. The effectiveness of SPC can be highlighted as follows: (i) ultrasound, through acoustic cavitation, provides an extra source of OH. from cavitation; (ii) acoustic cavitation can remove intermediates from the photocatalytic active sites. Acoustic cavitation generates a number of physical effects, such as shear forces, turbulence and micro-streaming, that help regenerate the active catalytic surface; (iii) when the catalyst or the pollutant is in the form of a powder or an agglomerate, acoustic cavitation increases the uniformity of the dispersion, thereby increasing the available surface area; (iv) acoustic cavitation is able to enhance mass transfer towards the liquid–solid interface; (v) acoustic cavitation is capa-

ble of accelerating the adsorption activity of reactant on the photocatalyst; and (vi) sonolysis is likely to decompose the hydrophobic part of the pollutant compound, which is unlikely to occur on the surface of the photocatalyst.

However, the combined use of photocatalysis and sonolysis for the treatment of pollutants is rather limited, mostly due to the lack of a detailed mechanism for this hybrid process. Most publications in this field deal with the degradation kinetics of the parent organic pollutants as a function of operation conditions. Relatively little is known about the reaction of by-products and pathway associated sonophotocatalytic treatment, since the product analysis plays a critical role in exploring and understanding the mechanism of this combined system and establishing a framework for its further application.

Methyl orange (MO), a typical azo dye, was selected as an organic pollutant in this study. Several recent studies [16–20] on the sonophotocatalytic treatment of MO showed it to be a very promising potential application of the hybrid system. However, all of these publications have mainly focused on the influence of various catalysts on the primary degradation of the parent organic pollutants. To the best of our knowledge, the identification and further degradation of the products during sonophotocatalytic degradation of methyl orange have not been studied to date.

In the present work, the degradation of both MO and its derivative products were systematically examined. A key aspect of this study is the evaluation of the degradation behavior of subsequent products formed during photocatalytic, sonochemical and sonophotocatalytic

* Corresponding author. Tel.: +61 3 93475180; fax: +61 3 83447090.
E-mail address: masho@unimelb.edu.au (M. Ashokkumar).

degradation of MO. We have found that there is a synergistic degradation of the intermediate products formed leading to a higher mineralization efficiency during the combined process.

2. Experimental details

2.1. Chemicals

All chemicals were purchased from commercial sources and used without further purification. MO was purchased from Tokyo Chemical Company. For each degradation experiment, a 250 mL aqueous solution containing 100 µM MO was used as the initial solution. Perchloric acid ($HClO_4$) and sodium hydroxide (NaOH), purchased from Ajax FineChem, were used to adjust the solution pH. A series of different concentrations of acid and alkaline solutions were made to control the solution pH. Degussa P25 TiO_2 with a specific surface area of 57 $m^2 g^{-1}$ was used as the photocatalyst. The loading of the photocatalyst was 1 mg mL^{-1} for all experiments. The ultra pure water (>18.6 MΩ cm^{-1} at 25 °C) used in the preparation of the aqueous solutions was sourced from a Milli-Q system (Millipore).

2.2. Degradation experiments

Sonophotocatalytic experiments were conducted in a 250 mL cylindrical Pyrex vessel with a quartz plate on one side. The sonication vessel contained a jacket, allowing the solution to be cooled (23 ± 3 °C) with cold water. An ultrasound transducer (213 kHz) was placed at the bottom of the vessel and the power absorbed by the solution was fixed at 55 mW mL^{-1} for all experiments, as measured by calorimetry. All experiments were carried out in an air atmosphere. It is known that sonication of water in air atmosphere generates nitric acid. However, we deliberately added perchloric acid and sodium hydroxide in order to maintain the solution pH at 2 and pH 10, respectively. Hence, the pH change due to nitric acid formation was not an issue in our experiments.

A 450 W Oriel Model 66021 xenon-arc lamp was used as the light source for the photocatalytic degradation experiments. An optical filter (cut-off wavelength 320 nm) was installed between the vessel and the lamp. During photocatalysis, the sonicator was switched off. Sonolysis experiments were carried out without light irradiation, but in the presence of the TiO_2 photocatalyst. During sonophotocatalysis, the solution was irradiated with both light and ultrasound.

Before each experiment was conducted, the solution was stirred with an overhead stirrer for 30 min to disperse the photocatalyst and to allow adsorption equilibrium of the dye to be reached on the TiO_2 surface. During the whole degradation experiment, the stirring speed was kept constant at 400 rpm and a bench top pH meter was used to monitor the solution pH.

Prior to analysis, all samples were filtered through a 0.45 µm filter to remove the suspended TiO_2 particles.

2.3. Analytical determinations

The progress of MO degradation was regularly monitored by UV–visible absorption using a Varian spectrophotometer (Cary Bio50). A computer controlled high performance liquid chromatography (HPLC) system (Shimadzu LC-10 AT VP system) comprising a solvent delivery pump, UV–visible diode array detector and an auto-sampler was used to characterize the organic pollutants and the by-product concentration–time profiles. The detector wavelength range was set from 190 to 640 nm. To qualitatively and quantitatively analyze the formation of the by-products, fractions were separated on an Alltech Econosphere C18 5 µm,

150 mm × 4.6 mm HPLC column. The mobile phase consisted of methanol and 10 mM ammonium acetate (30/70 v/v). The flow rate of the mobile phase was 1.0 mL min^{-1}.

The mineralized carbon was measured using a Shimadzu Total Organic Carbon (TOC) Analyzer, model TOC-V$_{CSH}$ equipped with an ASI-V autosampler. All the experiments were performed in duplicate, unless the maximum standard deviation or maximum coefficient of variation was exceeded, in which case additional measurements were conducted. A maximum standard deviation of 0.1 and a maximum coefficient of variation of 2% were set as acceptable criteria.

Mass spectrometry (MS) and LC/MS were performed on an Agilent Technologies 6510 Accurate-Mass Q-TOF coupled with an Agilent 1100 Series HPLC system. Chromatographic separation of the degradation products was performed using an Eclipse Plus C18 column (Agilent Technologies, 50 mm × 4.6 mm). The instrument was calibrated using an automatic tuning procedure with respective standard compounds. The mass spectra were recorded between m/z 25 and 100 in Auto MS/MS mode. The gas temperature was set at 325 °C and the collision energy was set to increase linearly with a 2 V/100 Da and 10 V offset. Mass profiles were acquired by Aiglent MassHunter Workstation Software Acquisition and processed using Agilent MassHunter Workstation Software Qualitative Analysis.

3. Results and discussion

3.1. Photocatalytic, sonolytic and sonophotocatalytic degradation

The chromatograms of MO during the sonophotocatalysis changes were observed as shown in Fig. 1. Similar chromatograms were collected for the sonolytic and photocatalytic experiments. Fig. 1 shows a clear decrease in the concentration of MO with increasing irradiation time.

A comparison of the degradation rate constants of MO observed for the different AOPs and for different solution pH values is shown in Fig. 2. A pseudo-first order kinetics model (Eq. (1)) was applied to compare the degradation performance of the three advanced oxidation processes under the chosen experimental conditions.

$$\ln \frac{C_0}{C_t} = kt \tag{1}$$

Where, C_0 is the initial concentration of the degradation reactant; C_t is the concentration at time t; k is the rate constant. The pseudo-first order kinetics is based on the assumption that the
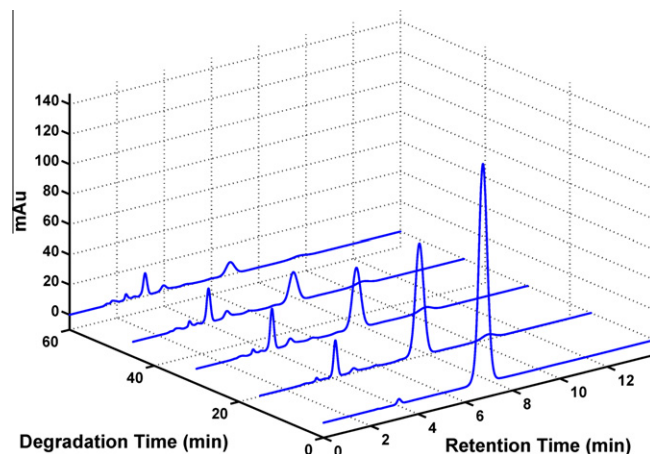

Fig. 1. 3D chromatographs observed during 60 min sonophotocatalytic degradation of 100 µM MO at pH 2. The TiO_2 was 1 mg mL^{-1}. The ultrasonic frequency was 213 kHz and the power was 55 mW mL^{-1}. The detection wavelength was 464 nm for monitoring the MO concentration.
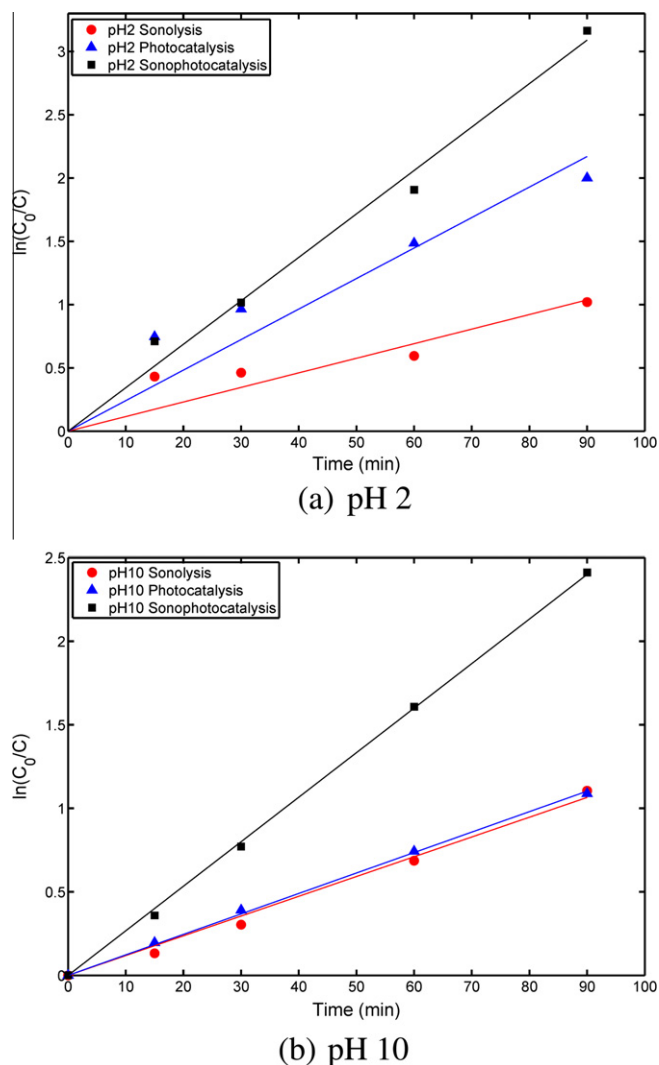
Fig. 2. Influence of pH on the degradation kinetics during the sonolysis, photocatalysis and sonophotocatalysis of an aqueous solution containing 100 µM MO. The TiO$_2$ loading in the oxidation system was 1 mg mL^{-1}. The applied ultrasonic frequency was 213 kHz and the power was 55 mW mL^{-1}. The detection wavelength used with HPLC was 464 nm.

Table 1
The pseudo first-order rate constants of sonolysis, photocatalysis and sonophotocatalysis of 100 µM MO in aqueous solution at pH 2 and pH 10.

pH Value	pH 2			pH 10		
Process	Sono	Photo	Sonophoto	Sono	Photo	Sonophoto
k (10^{-2} min^{-1})	1.2	2.4	3.4	1.2	1.2	2.7
Synergistic index		0.9			1.1	

all the samples at both pH 2 and pH 10 were adjusted to above 12 prior to analysis. A separate adsorption experiment showed that the minimum adsorption of MO occurred on the TiO$_2$ above pH 12. It is clearly seen that there is no significant influence of pH on the sonolysis of MO. Generally, due to the different ionic forms of acid–base organic molecules, and consequently different surface activities at different pH values, the sonochemical degradation exhibits a pH-dependent rate constant [22,23]. The slight difference in the rate constants obtained at the two different solution pH values implies there is not a large difference in the bubble/solution surface activity between the anionic and zwitterionic forms of MO.

From Table 1, the rate constant for the photocatalytic degradation of MO at pH 2 is almost twice that obtained at pH 10. According to the generally accepted mechanism of photocatalysis, the overall degradation efficiency is determined by the competition between the photo-generated recombination of free charge–carriers and trapping of the charged carriers by the surface adsorbed organic pollutants. At pH 2, due to the electrostatic attraction of positively charged TiO$_2$ and the negative charge of the zwitterionic dye, the adsorption of the dye at the semiconductor/solution interface is facilitated [24].

The faster sonophotocatalytic degradation at pH 2 is most likely due to the same mechanism that is responsible for the photocatalytic component of the process. Moreover, at both solution pH values, it is clearly seen from Table 1 that there is no apparent synergistic effect in the combined system. At both pH values, the sonophotocatalytic system shows an additive effect. As heterogeneous photocatalysis and ultrasonic irradiation initialize degradation of organic pollutants by reaction with OH. radicals [2,22], it therefore appears that under the conditions of the experiments both AOPs generate equivalent quantities of OH. radicals, irrespective of the presence of each other.

initial degradation reaction step is OH. attack on the dye molecule [2,22] and during the whole degradation process, the production of OH. radicals remains constant and reacts only with the organic pollutant. However, as the degradation products build up in solution, they could compete with MO for OH. radicals [21].

Here, in order to investigate the influence of pH and individual oxidation process, the data for the first 90 min was selected and used to calculate the rate constants as listed in Table 1.

At both pH 2 and pH 10, it is obvious that the sonophotocatalytic process is faster than the non-hybrid AOP degradation. Table 1 lists the experimentally obtained rate constants based on a pseudo-first order treatment of the data (Eq. (1)). The ratio of the sonophotocatalytic rate constant to the sum of the rate constants of the individual processes was used to evaluate the synergistic effect of the combined system as shown in Eq. (2).

$$\text{Synergistic Index} = \frac{k_{\text{sonophoto}}}{k_{\text{sono}} + k_{\text{photo}}} \qquad (2)$$

where, $k_{sonophoto}$, k_{sono} and k_{photo}, are the rate constants for sonophotocatalysis, sonolysis and photocatalysis, respectively. In order to reduce the influence of pH on the adsorption of MO onto TiO$_2$,
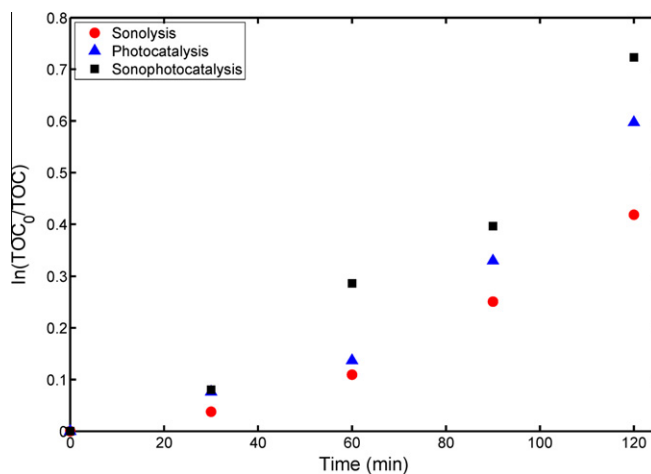

Fig. 3. Changes in TOC observed as a function of irradiation time during the photocatalytic, sonochemical and sonophotocatalytic degradation of 100 µM MO at pH 2 in aqueous solution. The TiO$_2$ loading in photocatalytic and sonophotocatalytic process was 1 mg mL^{-1}. The ultrasonic frequency was 213 kHz and the power was 55 mW mL^{-1}.

Fig. 3 shows the TOC content of aqueous solutions containing MO during the sonochemical, photocatalytic and sonophotocatalytic degradation processes at pH 2. It is obvious that the TOC in all systems gradually decreases with an increase in irradiation time, but not quite obeying first-order kinetics over the whole time range examined. The photocatalytic and sonochemical oxidation processes can effectively mineralize the azo dye. It can be seen that the combined system has a higher mineralization efficiency compared to the individual processes. However, as in the degradation of the parent compound, the overall mineralization is lower than an additive effect of the individual processes (negative synergistic effect).

3.2. Proposed sonophotocatalytic degradation pathway

The chromatograms of MO after 60 min sonolysis, photocatalysis and sonophotocatalysis at pH 2 are presented in Fig. 4. The chromatograms show clearly the appearance of peaks corresponding to the by-products from the degradation of the parent MO. It is evident that the same by-products were formed during all three AOPs. After 60 min degradation, nearly 70% of the MO was removed by photocatalysis (Fig. 4a), 50% by sonolysis (Fig. 4b) and 80% by sonophotocatalysis (Fig. 4c). However, according to Fig. 4, after 60 min, many intermediate species were still present in the solution. There are seven main products (**A**–**G**) observed in the chromatographs of all three AOPs. The peak corresponding to the remaining MO decreases in the following order: sonophotocatalysis < photocatalysis < sonolysis. These observations indicate that the photocatalytic and sonophotocatalytic degradation processes are the more efficient processes in decomposing the parent azo dye. This observation corresponds to the UV–vis spectra, kinetics results and TOC analysis. Additionally, the by-products include hydrophobic as well as hydrophilic intermediate compounds. As mentioned previously, the solvophyllic nature of the compound favours differing processes during sonophotocatalytic degradation. The hydrophobic products tend to be surface active at the bubble/solution interface and therefore more readily degraded by acoustic cavitation. However, photocatalysis has a greater capability to decompose the hydrophilic products.

The molecular structures of the by-products were deduced by analyzing the samples with MS, MS/MS and comparing the results from the literature [25–29]. The parent molecule, MO (retention time: 8.4 min), exhibits a clear MS signal corresponding to a negative ion m/z 304. It is worth noting that one intermediate among these seven products, **G**, exhibited a longer retention time (m/z 320, retention time: 12.8 min) indicating greater hydrophobicity. Normally, hydroxylated products show a more hydrophillic character. Despite this contradiction, it was confirmed that product **G** was a monohydroxylated MO. The same hydrophobic hydroxylated product has been observed in photocatalysis by a number of research groups [25–27,29].

Product **D** (m/z 290, retention time: 3.6 min) is a demethylated intermediate formed by cleaving a methyl group from the MO molecule. The remaining intermediate compounds are by-products formed by the addition of one or two hydroxyl groups or cleavage of one or two methylene groups. For example, Product **B** (m/z 292, retention time: 2.4 min) is a derivative formed by addition of one hydroxyl group and extraction of two methyl groups from the MO molecule.

Based on the structures of the by-products formed during the degradation, all the identified intermediates contain both the azo group and the sulfonic group. The structures of these intermediates were further confirmed by UV–vis spectroscopy.

As shown in the list of by-products (Fig. 4), the molecules formed during the sonolytic, photocatalytic and sonophotocatalyt-
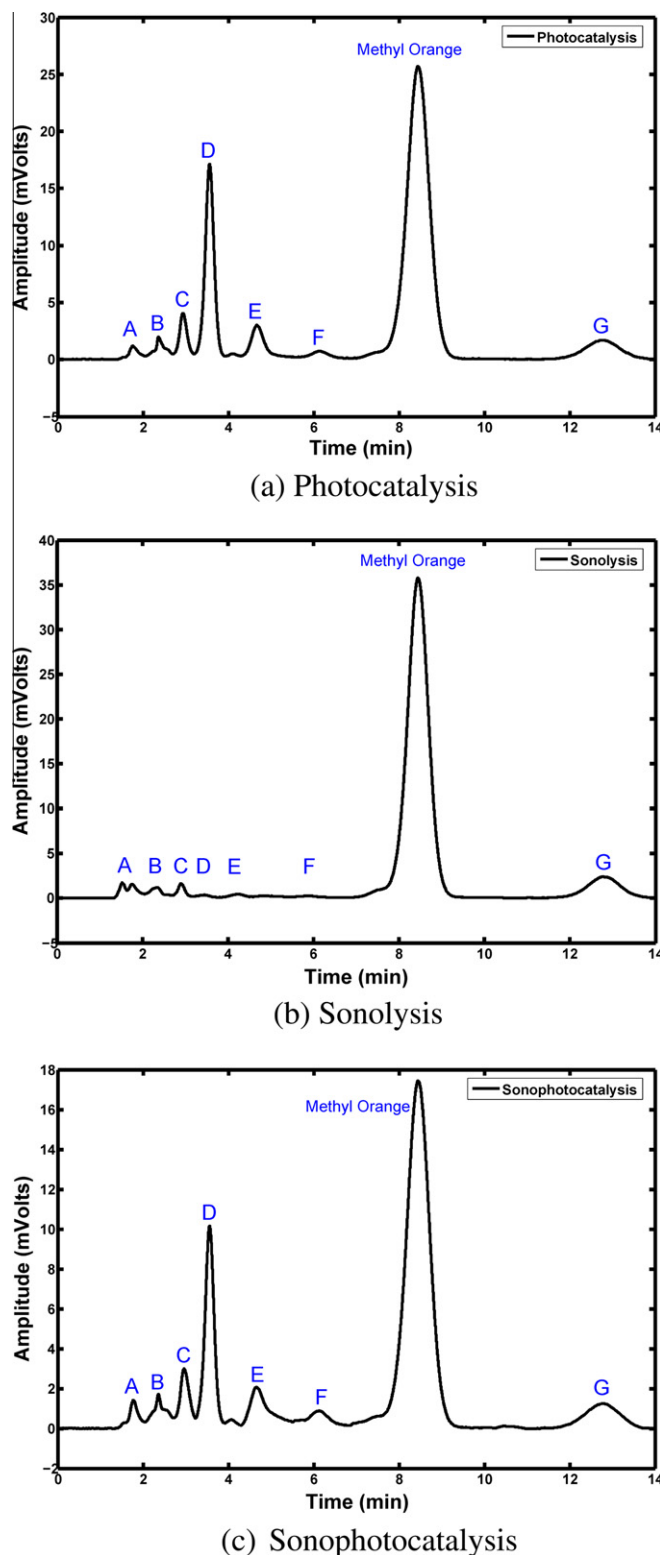

(a) Photocatalysis

(b) Sonolysis

(c) Sonophotocatalysis

Fig. 4. High performance liquid chromatographs observed after 60 min of photocatalytic, sonolytic and sonophotocatalytic degradation of 100 μM MO at pH 2. The TiO$_2$ loading in all three oxidation systems was 1 mg mL^{-1}. In sonolysis and sonophotocatalysis, the ultrasonic frequency was 213 kHz and the power was 55 mW mL^{-1}. The detection wavelength range of 3D chromatographs was 190–640 nm and 464 nm for monitoring MO concentration.

ic degradation of MO originated from the hydroxylation and/or demethylation of MO. Fig. 5 shows a proposed sonophotocatalytic degradation pathway scheme. The degradation pathway mainly
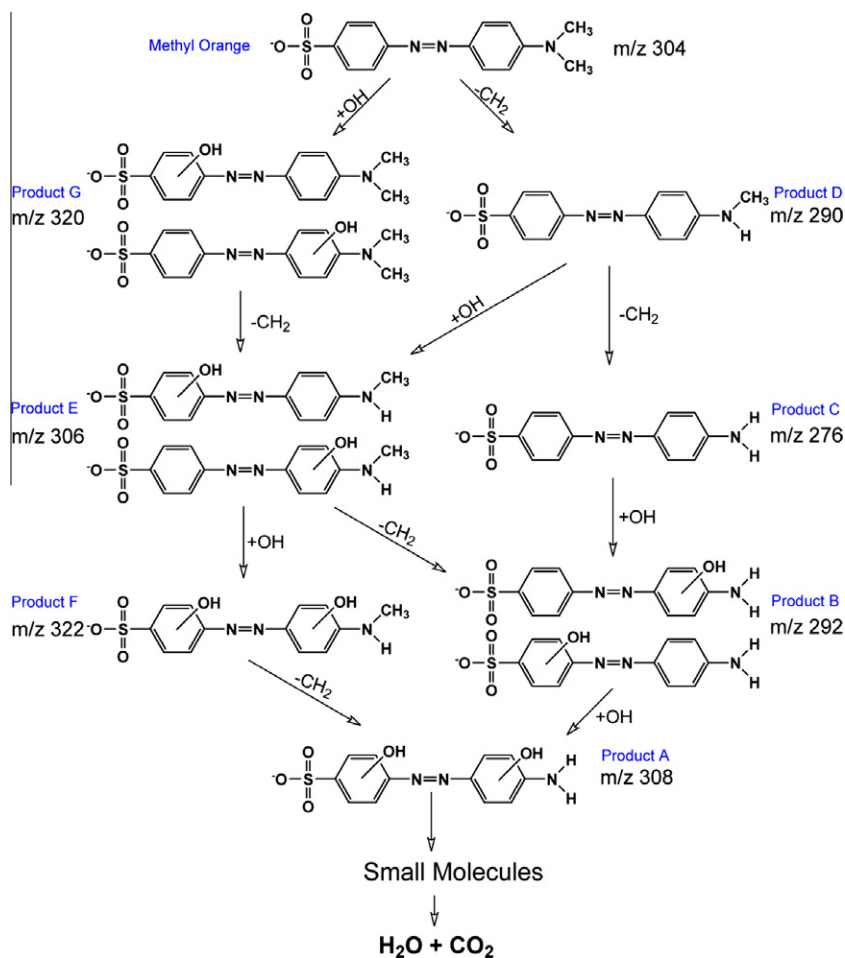
Fig. 5. Schematic illustration of the proposed degradation pathway and the events taking place during the sonophotocatalytic degradation of MO.

focuses on the transformation of the intermediate species, which precedes the aromatic ring-opening.

Products **D** and **G** are intermediate compounds formed through the demethylation and hydroxylation of MO, respectively (Fig. 5). The demethylation of MO is a process which involves the homolytic rupture of the nitrogen-carbon bond of the amine group leading to the substitution of a methyl group with a hydrogen atom. Consecutive demethylation is the likely pathway to the formation of Products **E** and **B**. Whichever decomposition process MO molecules undergo, sonolysis or photocatalysis, OH• radical attack is the main cause of degradation [2,22]. Products **A**, **B**, **E** and **G** are formed by multiple substitutions of hydroxyl groups. Evidently, due to simultaneous and independent occurrences, both demethylation and hydroxylation can be expected to couple with each other or take place alternatively. Consequently, the by-products of MO degradation are determined by the individual demethylation and hydroxylation processes, and by their combinations.

3.3. Degradation of by-products

Two primary intermediate by-products, Product **D** (a demethylated product) and Product **G** (a monohydroxylated product) were monitored in order to investigate the sonochemical, photocatalytic and sonophotocatalytic degradation of the intermediate products. Fig. 6 shows the HPLC peak areas for these two intermediates as a function of the irradiation time. The peak areas of both by-products at different pH values first increase and subsequently de-

crease, demonstrating that they undergo two processes: formation and decomposition.

Fig. 6a shows the formation trend of Product **D** as a function of irradiation time during sonolysis, photocatalysis and sonophotocatalysis. The peak areas in both photocatalysis and sonophotocatalysis show a bell shape trend with irradiation time. The amount of Product **D** formed during both processes reaches its maximum within the first 30 min. However, the amount of Product **D** existing in solution gradually increases over the whole sonochemical degradation process. This observation demonstrates that the decomposition is faster than the formation during photocatalytic and sonophotocatalytic degradation, and the hybrid technique is better for decomposing the intermediate **D**. The destruction of the intermediate by sonolysis seems to be the slowest among these three advanced oxidation processes. Compared to pH 2, the amount of Product **D** formed at pH 10 is considerably larger (shown in Fig. 6b), indicating that in spite of the formation of the same main active species, the pH environment is capable of changing the proportion of products formed. Consequently, it is possible to choose the right process and pH conditions in order to inhibit the formation of certain products, which may also be harmful to the environment. At pH 10, the amount of Product **D** during the sonophotocatalytic process reaches a maximum at 30 min, but in photocatalysis it is at 90 min. At pH 10, the hybrid system exhibits a greater synergistic effect for the degradation of Product **D** than that at pH 2.

Fig. 6c and d show the change in amount of Product **G** with irradiation time under the three AOPs at pH 2 and pH 10, respectively.
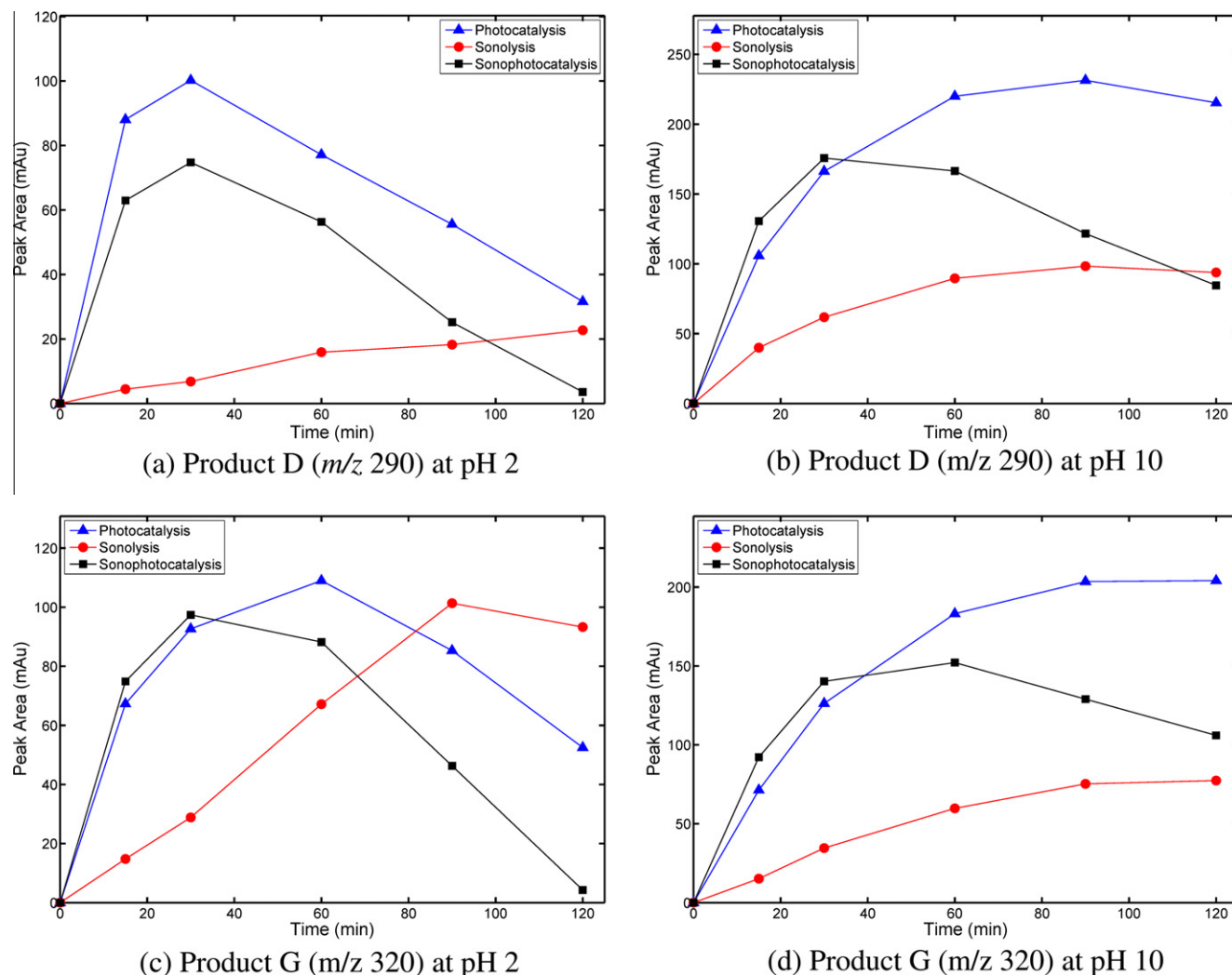
Fig. 6. The concentration changes of Products D and G during 120 min sonophotocatalytic degradation of 100 μM MO at pH 2 and pH 10. The TiO$_2$ loading in each experiment was 1 mg mL^{-1}. In the sonolysis and sonophotocatalysis processes, the frequency of ultrasound was 213 kHz and the power was 55 mW mL^{-1}.

The hydroxylation of MO in photocatalytic and sonophotocatalytic processes is faster than under sonolysis. During the first 30 min at pH 2, MO was hydroxylated by photocatalysis at the same rate as sonophotocatalysis. However, after 30 min, the amount of mono-hydroxylated product in sonophotocatalysis decreased while that in photocatalysis increased until 60 min. The reason for the faster sonophotocatalytic decomposition of Product **G** may lie in the sonochemical pathway. Compared to Product **D**, Product **G** exhibits a greater hydrophobicity (HPLC chromatograph in Fig. 4), leading to a higher bubble/solution surface activity. This property allows these molecules to accumulate at the liquid/bubble interface and thus increases their exposure to the primary radicals generated within the cavitation bubbles.

The maximum amounts of Products **D** and **G** are higher at pH 10 than that at pH 2. One possible reason is that the alkaline environment favours the formation of OH**.** radicals and consequently facilitates the hydroxylation process.

4. Conclusions

The results reported here demonstrate that sonophotocatalysis is an effective technique for environmental remediation. A lower solution pH environment facilitates the sonophotocatalytic degradation of MO in aqueous solution. The pH and the physico-chemical properties of the organic species affect their hydrophobicity and therefore their surface active properties. These changes contribute to changes in the overall sonophotocatalysis rate. Furthermore, it has been demonstrated that the solution pH can affect the build-up rate of each by-product generated during sonolysis, photocatalysis and sonophotocatalysis. It was found that sonophotocatalytic degradation of the parent organic pollutant, as well as the derivative by-products, was much faster than the individual oxidation processes combined. In particular, it has been demonstrated that sonophotocatalysis was significantly more effective at degrading the intermediate by-products. Therefore, the sonophotocatalytic technique is likely to lead to both a more complete and a faster mineralization of organic pollutants in aqueous solutions than the individual processes. It was observed that sonolysis is effective in decomposing hydrophobic organic compounds and photocatalysis is better for hydrophilic compounds. The hydrophobic quality of a solute leads to a higher surface activity of the molecules and results in enhancing the encounters between the organic molecules and the highly reactive primary radicals at the liquid/bubble interface. Hydrophilic molecules on the other hand are more readily adsorbed onto the surface of TiO$_2$ and decomposed by photocatalysis. The results shown in this paper are also significant in understanding the sonophotocatalytic degradation

activities and provide information related to the decomposition pathway of organic dye molecules.

References

[1] O. Carp, C.L. Huisman, A. Reller, Photoinduced reactivity of titanium dioxide, Prog. Solid State Chem. 32 (2004) 33–177.

[2] A. Fujishima, K. Hashimoto, T. Watanabe, Photocatalysis: Fundamentals and Applications, 1st ed., BKC Inc., Tokyo, 1999.

[3] A. Fujishima, T.N. Rao, D.A. Tryk, Titanium dioxide photocatalysis, J. Photochem. Photobiol., C 1 (2000) 1–21.

[4] M.R. Hoffmann, S.T. Martin, W. Choi, D.W. Bahnemann, Environmental applications of semiconductor photocatalysis, Chem. Rev. 95 (1995) 69–96.

[5] Y.G. Adewuyi, Sonochemistry in environmental remediation. 1. Combinative and hybrid sonophotochemical oxidation processes for the treatment of pollutants in water, Environ. Sci. Technol. 39 (2005) 3409–3420.

[6] Y.G. Adewuyi, Sonochemistry in environmental remediation. 2. Heterogeneous sonophotocatalytic oxidation processes for the treatment of pollutants in water, Environ. Sci. Technol. 39 (2005) 8557–8570.

[7] M. Ashokkumar, F. Grieser, Untrasound assisted chemical process, Rev. Chem. Eng. 15 (1999) 41–83.

[8] M. Ashokkumar, T.J. Mason, Sonochemistry, in: Kirk–Othmer Encyclopedia of Chemical Technology, John Wiley & Sons, New Jersey, 2007.

[9] V. Augugliaro, M. Litter, L. Palmisano, J. Soria, The combination of heterogeneous photocatalysis with chemical and physical operations: A tool for improving the photoprocess performance, J. Photochem. Photobiol., C 7 (2006) 127–144.

[10] J. Madhavan, F. Grieser, M. Ashokkumar, Combined advanced oxidation processes for the synergistic degradation of ibuprofen in aqueous environments, J. Hazard. Mater. 178 (2010) 202–208.

[11] J. Madhavan, P.S. Sathish Kumar, S. Anandan, F. Grieser, M. Ashokkumar, Sonophotocatalytic degradation of monocrotophos using TiO_2 and Fe^{3+}, J. Hazard. Mater. 177 (2010) 944–949.

[12] B. Neppolian, L. Ciceri, C. Bianchi, F. Grieser, M. Ashokkumar, Sonophotocatalytic degradation of 4-chlorophenol using $Bi_2 O_3/TiZrO_4$ as a visible light responsive photocatalyst, Ultrason. Sonochem. 18 (2010) 135–139.

[13] P.R. Gogate, A.B. Pandit, Sonophotocatalytic reactors for wastewater treatment: A critical review, AIChE J. 50 (2004) 1051–1079.

[14] J. Madhavan, F. Grieser, M. Ashokkumar, Degradation of orange-G by advanced oxidation processes, Ultrason. Sonochem. 17 (2010) 338–343.

[15] J. Peller, O. Wiest, P.V. Kamat, Synergy of combining sonolysis and photocatalysis in the degradation and mineralization of chlorinated aromatic compounds, Environ. Sci. Technol. 37 (2003) 1926–1932.

[16] N. Bejarano-Perez, M. Suárez-Herrera, Sonophotocatalytic degradation of congo red and methyl orange in the presence of TiO_2 as a catalyst, Ultrason. Sonochem. 14 (2007) 589–595.

[17] H. Wang, J. Niu, X. Long, Y. He, Sonophotocatalytic degradation of methyl orange by nano-sized Ag/TiO_2 particles in aqueous solutions, Ultrason. Sonochem. 15 (2008) 386–392.

[18] S. Wang, Q. Gong, J. Liang, Sonophotocatalytic degradation of methyl orange by carbon nanotube/TiO_2 in aqueous solutions, Ultrason. Sonochem. 16 (2009) 205–208.

[19] K. Wantala, D. Tipayarom, L. Laokiat, N. Grisdanurak, Sonophotocatalytic activity of methyl orange over Fe (III)/TiO_2, React. Kinet. Catal. Lett. 97 (2009) 249–254.

[20] Z. Zhang, Y. Yuan, L. Liang, Y. Fang, Y. Cheng, H. Ding, G. Shi, L. Jin, Sonophotoelectrocatalytic degradation of azo dye on TiO_2 nanotube electrode, Ultrason. Sonochem. 15 (2008) 370–375.

[21] K. Okitsu, K. Iwasaki, Y. Yobiko, H. Bandow, R. Nishimura, Y. Maeda, Sonochemical degradation of azo dyes in aqueous solution: A new heterogeneous kinetics model taking into account the local concentration of OH radicals and azo dyes, Ultrason. Sonochem. 12 (2005) 255–262.

[22] R. Singla, F. Grieser, M. Ashokkumar, The mechanism of the sonochemical degradation of benzoic acid in aqueous solutions, Res. Chem. Intermed. 30 (2004) 723–733.

[23] R. Singla, F. Grieser, M. Ashokkumar, Sonochemical degradation of martius yellow dye in aqueous solution, Ultrason. Sonochem. 16 (2009) 28–34.

[24] N. Guettai, H. Ait Amar, Photocatalytic oxidation of methyl orange in presence of titanium dioxide in aqueous suspension. Part I: Parametric study, Desalination 185 (2005) 427–437.

[25] C. Baiocchi, M.C. Brussino, E. Pramauro, A.B. Prevot, L. Palmisano, G. Marci, Characterization of methyl orange and its photocatalytic degradation products by HPLC/UV-vis diode array and atmospheric pressure ionization quadrupole ion trap mass spectrometry, Int. J. Mass Spectrom. 214 (2002) 247–256.

[26] R. Comparelli, E. Fanizza, M.L. Curri, P.D. Cozzoli, G. Mascolo, R. Passino, A. Agostiano, Photocatalytic degradation of azo dyes by organic-capped anatase nanocrystals immobilized onto substrates, Appl. Catal., B 55 (2005) 81–91.

[27] K. Dai, H. Chen, T. Peng, D. Ke, H. Yi, Photocatalytic degradation of methyl orange in aqueous suspension of mesoporous titania nanoparticles, Chemosphere 69 (2007) 1361–1367.

[28] J.M. Joseph, H. Destaillats, H.M. Hung, M.R. Hoffmann, The sonochemical degradation of azobenzene and related azo dyes: rate enhancements via Fenton's reactions, J. Phys. Chem. A 104 (2000) 301–307.

[29] A.B. Prevot, A. Basso, C. Baiocchi, M. Pazzi, G. Marcí, V. Augugliaro, L. Palmisano, E. Pramauro, Analytical control of photocatalytic treatments: degradation of a sulfonated azo dye, Anal. Bioanal. Chem. 378 (2004) 214–220.